공학석사학위논문

펄스 에너지원을 구동력으로 하는 균일 유동 마이크로젯 인젝터 개발 및 응용 기술

Development and application of constant flow generating injector with pulse energy source as driving force

2018년 2월

서울대학교 대학원

기계항공공학부

함 휘 찬

펄스 에너지원을 구동력으로 하는 균일 유동 마이크로젯 인젝터 개발 및 응용 기술

Development and application of constant flow generating injector with pulse energy source as driving force

지도교수 여 재 익

이 논문을 공학석사 학위논문으로 제출함

2017년 11월

서울대학교 대학원
기계항공공학부
함 휘 찬

함휘찬의 공학석사 학위논문을 인준함

2017 년 12 월

위 원 장 ________ (인)

부위원장 ________ (인)

위 원 ________ (인)

Abstract

A narrow nozzle ejects a microjet of 150 μm in diameter with a velocity of 140 m/s a by the laser-induced bubble expansion in the designed injector. The pulsed form of the driving force at a period of 10 Hz from the connected Er:YAG laser makes it possible for multiple microjet ejections aimed at delivery of drugs into a skin target. The pulsed actuation of the microjet generation is however susceptible to the air leak which can cause the outside air to enter into the momentarily de-pressurized nozzle, leading to a significant reduction of the microjet speed during the pulsed administering of the drug. In the present study, we designed a ball-check valve injector which is less prone to an unwanted air build up inside the nozzle by controlling the nozzle pressure to remain above ambient pressure at all times. The new device is rigorously compared against the reported performance of the previous injector and has shown to maintain about 97% of the initial microjet speed regardless of the number of shots administered; likewise, the drug penetration depth into a porcine skin is improved to 1.5 to 2.25 times the previously reported penetration depths.

***Keywords*: Microjet; Laser-induced bubble; Ball-chenck valve; Needle-free; Drug-delivery; Jet injection**

***Student Number*: 2016-20759**

LIST

LIST OF TABLES

LIST OF FIGURES

CHAPTER 1

INTRODUCTION

Since the flow generation actuator is used as a component of many kinds of mechanical systems, its minimization of power loss and improvement of output efficiency are major issues. One of the most common types of flow generators is a pump. Pumps are used to move liquids or slurries in desired directions and destinations, and diverse forms of pumps have been developed. Reciprocating pump, rotary vane pump, and centrifugal pump are the main types of pump, and they all have a power source, which uses power source which outputs continuous power [1-3]. The continuous power source means a power source in which the power output is not zero but is continuous in order to actuate the machine. However, typical conventional pumps introduced above operate using only continuous power from combustion engines, electric motors, and physically powered motors. In addition to this continuous power source, a power source providing a pulse type output has been developed to date. For example, a high-powered pulsed laser, electromagnetic pulse [4], and the like are power sources providing a pulsed output. This power source has the advantage of emitting a large amount of peak power to the load by releasing the stored energy over a short interval. Therefore, it seems that the actuator that requires high-pressure or high-energy density flow can be designed when the mechanism that transfers the fluid through this power source is implemented.

An example of a flow generator that can be implemented through a pulsed power source is the microjet drug delivery system using pulsed

laser-induced bubble growth. A microjet drug delivery system in which a drug solution penetrates directly through the epidermis of the skin and penetrates into the body by high-speed injection of the drug solution into a micron-sized microjet has been investigated [4]. The laser-induced bubble growth type microjet injection method has been developed by the present inventions as shown in Fig. 1 [5-7] and it uses a pulsed laser irradiated at a 10 Hz, and the microjet-type drug is injected at the same period. According to the above-described microjet drug delivery device, when a strong energy such as a laser is intensively irradiated through the energy focusing unit to the pressure generating liquid in the pressure chamber, the pressure generating liquid evaporates instantaneously. So bubbles were generated and expand rapidly while the elastic membrane rapidly pushed the drug solution in the drug chamber out through the nozzle. The microjet ejection speed was sufficiently fast for transdermal injection of the drug [8,9].

But distinct from the bubbles generated via the laser irradiation in the pressure chamber, the growing air bubbles in the drug chamber nozzle could be observed. It is predicted that the cause of growing air bubbles in the drug chamber nozzle after a microjet ejection is due to the external air inflow. The external air inflow is stem from the decrease of the internal pressure of the drug chamber nozzle immediately after the drug injection. Due to the air inflows (the same volume as the injected drug), the air bubble gradually grows. Therefore, when the injection is continued, the pressure to be transferred from the pressure chamber to the drug is greatly reduced, so that the jetting property and the penetration performance of the micro jet are deteriorated.

Therefore, the present study was aimed at developing a mechanism to transport fluid in one direction with no inflow from outer air to operate a flow generator such as a microjet drug delivery system through a pulsed power source (pulsed laser). achieving maximum efficiency of repeated microjet performance via removing the air bubbles in the drug chamber nozzle. Specifically, the present study is focused on maintaining the injection performance of the microjet and the penetration of the skin irrespective of repetition of injection. More specifically, the penetration depth should be kept constant with repeated injections, and the penetration depth should reach at least 80% of the penetration depth performance of the original nozzle device. A ball-check valve having a mechanism for opening or closing the drug chamber nozzle is designed and introduced. The present paper is meaningful to show the possibility of developing a high-power flow releasing generator by applying a mechanism for implementing a flow generator using the pulse type power source to microjet drug delivery system. The key to such a mechanism is to control the flow of fluid through the introduction of a ball check valve and to automatically fill the chamber immediately after the flow corresponding to each pulse. In conclusion, the flow generated from the microjet drug delivery system using the ball check valve maintained the same performance even when the number of drug firing was repeated, and when the ball check valve developed in this study was applied, the penetration performance was improved as compared with the other systems. We also set variables that change the flow performance and found the parameters for performance optimization.

CHAPTER 2

Uniform microjet flow generation through check valve and its application technology

2.1 Materials and methods

Shown in Fig. 2.1 is the drug delivery system consisting of the upper pressure chamber filled with the water and the lower drug chamber nozzle that is separated from the upper unit via the elastic membrane. Additional drug reservoir connected to the nozzle via a syringe supplies the necessary dosage of the medicine. Er:YAG laser of 2.940 μm at 150 μs pulse duration is used to irradiate the water of upper pressure chamber having the best absorption coefficient in water (~ 15,000 1/cm-1) [10].

2.1.1 Pressure chamber and drug nozzle in contact with the elastic membrane

Inside the microjet injector, the driving force for microjet injection propulsion of the drug solution is generated from the working fluid filled in the pressure chamber, and the laser energy is irradiated at the working fluid so that it is vaporized and bubbles are generated in the liquid. The vapor bubble generated in the working fluid instantaneously expands and disappears when irradiation of the laser is stopped. The rapid expansion of the bubble causes the elastic film to elongate outward toward the drug chamber nozzle transferring a pressure load

onto the drug chamber nozzle. The resulting microjet speed reaches well above 100 m/s, ejecting from a nozzle diameter ranging from 150 to 300 μm.

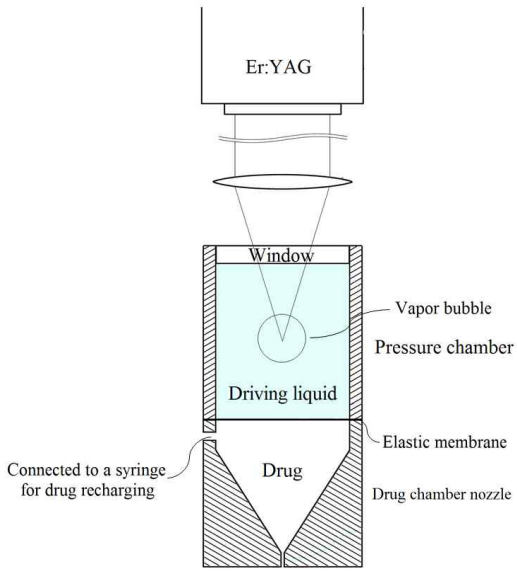

Fig. 2.1. Schematics of drug chamber nozzle attached to a pressure chamber

2.1.2 Newly designed ball-check valved drug chamber nozzle

Figure 2 depicts how the drug chamber nozzle is designed with a ball-check valve that governs the open or closure of flow between the two regions. The ball-check valve is open while ejecting the microjet out of the nozzle due to an elastic expansion of the membrane. Then the membrane retracts upon elastic restoration of the potential energy associated with laser-induced bubbles in the driving pressure chamber, and the ball-check valve closes. The check valve contains a space on

which reciprocating ball seats through spring tension. The ball has a diameter larger than the valve for a sealed closure of the valve with the necessary stiffness of the spring.

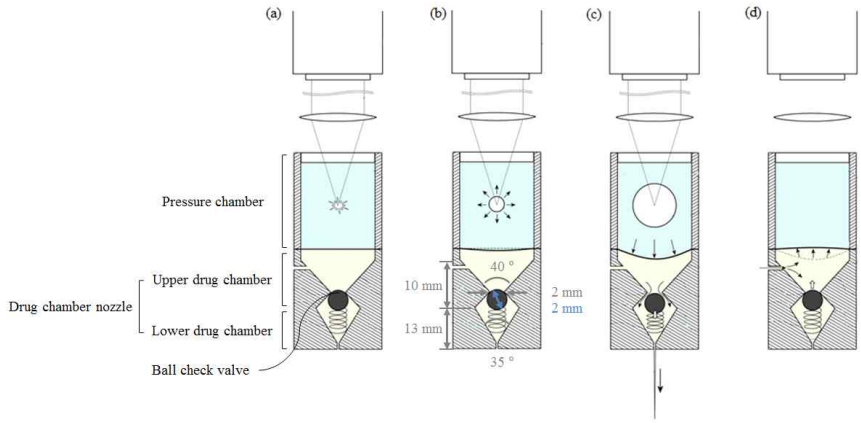

Fig. 2.2. Schematics of newly designed injector utilizing a ball-check valve. (a) laser beam irradiated; (b) vapor bubble growth by focused laser beam; (c) opened nozzle and drug flows through the neck; (d) closed nozzle and drug is refilled from syringe-type drug reservoir

2.1.3 Measurements of jet speed and ball motion

In this study, one of the criteria for assuring a consistency of the performance of the system regardless of the number of injections is the steady microjet speed. The jet speed is measured by using the high-speed camera (Phantom v711). The image is recorded at 49,026 fps with a resolution of 112 x 600 for the jet speed. The movement of the ball and the trace particles (0.25 - 0.50 μm) inside the chamber is also measured at 40,000 fps with a resolution of 208×504. The actual measurement distance per pixel is calculated at the focal length of the

photographed image and the speed is obtained. The jet speed is measured at an instant when the jet first leaves the nozzle.

2.1.4 Tissue targets

Another criterion for a stable performance of the drug delivery unit is the drug penetration depth in the porcine skin, irrespective of the number of shots fired. The porcine skins used in the target samples have ultimate tensile strength of 10-30 MPa with 20-30 μm of the stratum corneum thickness. The ultimate tensile strength of human skin is 2-15 MPa, which is less than the porcine tissue sample used in this study [10,11]. Nevertheless, the porcine skin has similar morphology and layer structure as human skin. We fixed the treated tissue samples in a 10% formaldehyde solution and then embedded in paraffin. The samples are sliced and stained with H&E (hematoxylin-eosin) dye. The photomicroscope (Axiophot) took the cross-sectional view of the skin.

2.2 Results and discussion

2.2.1 Adverse air inflow into nozzle causing injector performance degradation

Figure 2.3 shows images of the inside of the drug chamber nozzle taken at intervals of 6 seconds and for the entire duration of 60 seconds or 600 shots. Shown in (a) is the original nozzle without the check valve while (b) demonstrates the inside of the ball-check valve nozzle. With the number of shots increased, the air pocket grows significantly in (a) where the drug volume underneath the elastic membrane is taken up by the air. No air pocket formed inside the ball-check valve nozzle, irrespective of the number of microjets fired.

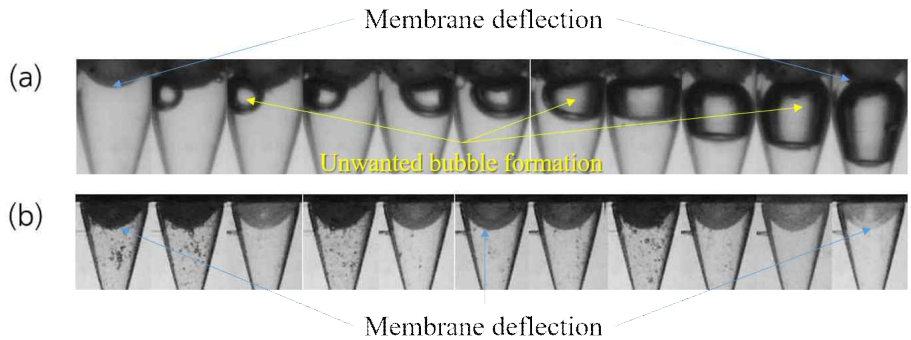

Fig. 2.3. Images of inside the drug nozzle taken at 6-second interval: (a) original nozzle is showing a growing air pocket and (b) check valve nozzle showing no air pocket (laser fluence of 87 J/cm2).

Figure 2.4 shows the microjet speed with respect to the number of shots. The triangular symbol represents the resulting microjet speed of a standard nozzle, and the square symbol is those of the valve nozzle.

As the number of shots increases, the air pocket growth in (a) becomes significant as such the jet speed degrades. Although the initial speed reaches 140 m/s, the rapid decrease is shown after about 150 shots and approaches 60 m/s, no longer suitable for skin penetration. On the other hand, the injector equipped with a ball-check valve maintains a constant speed of 140 m/s regardless of the number of shots tested. This steady performance is a clear proof that the successful removal of air pocket inside the drug nozzle is the reason for such excellent injector performance as presented.

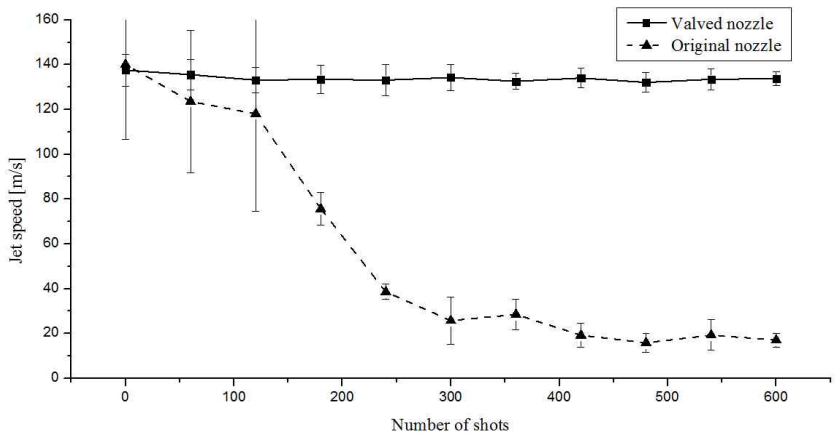

Fig. 2.4. Changes in the jet speed with the number of shots of micro jets. Each case of experiment was performed 10 times and the range of jet speed is indicated through the error bars.

Figure 2.5 shows the sequential images of microjet formation at the interval of 20.4 μs. The figure in (a) describes the process of microjet ejection from the ball-check valve injector, and the figure in (b) corresponds to the standard injector without the check valve. We obtained microjet speed of 143 m/s and 140 m/s in each injector, based

on 10 measurements. As for the resulting microjet shape, both showed well-focused and straight without any pre-atomization that might lead to inefficient penetration performance causing bruises and potential surface contamination.

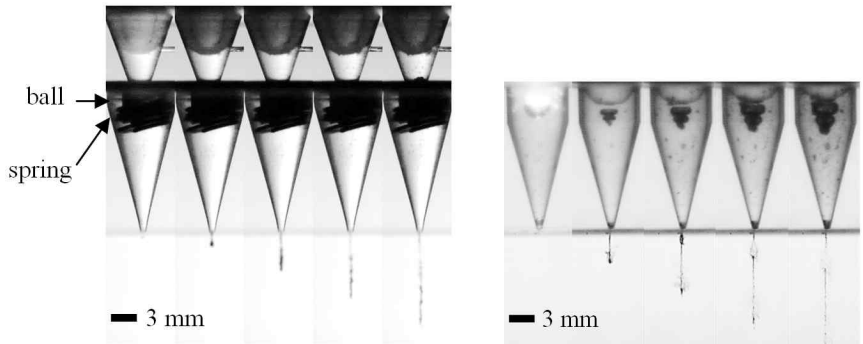

(a) **(b)**

Fig. 2.5. The sequential images of ejecting microjets at intervals of 20.4 μs using (a) valve nozzle and (b) no-valve nozzle injector (laser fluence of 87 J/cm2).

2.2.2 Penetration on porcine skins

Table 2.1 summarizes the drug penetration results into the stratum corneum of porcine skin shown with the cross-sectional view of the tissue. A blue tattoo ink was used to emphasize the visibility at the penetration site. The treatment time or the duration of injection was varied from 3 to 20 seconds to correlate the number of drug injections and the penetration performance. The nozzle with the valve showed a better performance as the injector administered more drug transdermally than the previous. The complete removal of the air pocket inside the

valve nozzle is the main reason for such performance enhancement.

Table 2.1. Comparison of the nozzles for drug penetration into the stratum corneum of a porcine skin (cross-sectional view)

Number of shots	Valve Nozzle	Original Nozzle	Scale
30			 4 mm
50	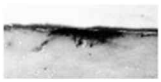	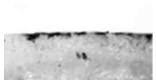	
90			
130			
200			

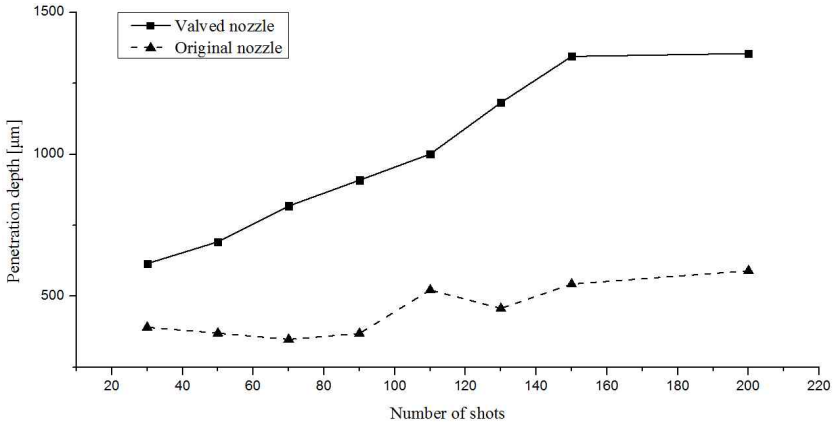

Fig. 2.6. Measured drug penetration depth in the porcine skin

Figure 2.6 is a graphical representation of the penetration results of Table 1. With the microjet speed remained constant regardless of the number of shots administered, the penetration depth also increased with a valve nozzle.

Fig. 2.7. Tattooed image of a tree on the porcine skin

Shown in Fig. 2.7, a tree image is crafted on the porcine skin by multiple injections of a tattoo ink.

2.2.3 External syringe-type drug reservoir

As shown in Fig. 2.8, the drug chamber is connected to a recharging unit or a syringe-type drug reservoir. There is an advantage that the drug solution is automatically moved according to the internal pressure fluctuation of the drug chamber due to the operation of the microjet injector without additional power means such as a separate micro pump.

By replenishing the same amount of drug as the drug, the internal pressure and the drug capacity of the drug chamber are restored to the pre-injection state, so that the inflow of air from the outside can be prevented and the continuous re-injection becomes possible. The external drug syringe used in this study is a 5 ml HSW syringe and has an internal radius of 6.25 mm.

The driving force that enables the drug to be automatically charged from the syringe-type drug reservoir to the drug chamber is the result of the difference between the pressure outside the syringe (the ambient air) and the pressure in the upper chamber. When this pressure difference pushes the piston of the syringe, a flow occurs inside the syringe. At this time, due to the viscosity of the syringe inner wall, the pressure difference $\Delta P_{syringe}$ from the surface of the piston to the entrance of the syringe nozzle occurs, and the pressure difference ΔP_{sc} is generated by 90 ° sudden contraction of the narrow nozzle entrance inside the syringe. The sum of $\Delta P_{syringe}$ and ΔP_{sc} is the pressure difference between the ambient air and the upper chamber, which causes the net force to pushes the piston of the syringe-type drug reservoir after drug escape the upper drug chamber.

If the flow is assumed to be incompressible viscous flow, the flow rate inside the syringe can be expressed as follows by applying the Poiseuille equation [11].

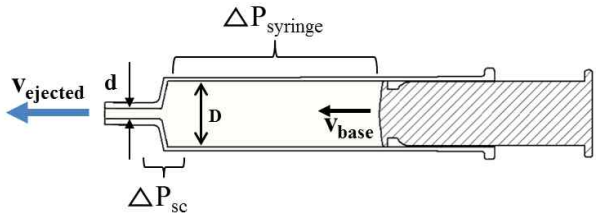

Fig. 2.8. The schematic of syringe-type drug reservoir

$$Q = \frac{\pi r^4 \Delta P}{8\eta L} \tag{2.1}$$

The flow rate is equal to the product of the cross sectional area of the syringe and the flow rate at the front of the piston. The pressure change by wall friction (from the surface of the piston to in front of the narrow entrance of nozzle) $\Delta P_{syringe}$ inside the syringe is as follows.

$$\Delta P_{syringe} = \frac{8\eta L A v_{base}}{\pi r^4} \tag{2.2}$$

Apply the momentum conservation law and the sudden contraction loss coefficient, K_{sc}, to obtain the pressure change by sudden contraction of the syringe (occurs when the drug flow passes through the the narrow entrance of the syringe's nozzle, diameter D to d) ΔP_{sc} applied to the flow in and out of the syringe [12].

$$\Delta P_{sc} = \frac{\rho v_{ejected}^2}{2} - \frac{\rho v_{base}^2}{2g} + K_{se}\frac{\rho v_{ejected}^2}{2} \tag{2.3}$$

At this time, the flow speed of the outlet $v_{ejected} = A_{base}/A_{ejected}v_{base}$ and the sudden contraction loss coefficient K_{sc} is as follows.

$$K_{sc} = 0.42\left(1 - \frac{d^2}{D^2}\right) \tag{2.4}$$

The pressure change by sudden contraction ΔP_{sc} is as follows.

$$\Delta P_{sc} = \frac{\rho}{2}\left(\frac{A_{base}^2}{A_{ejected}^2}v_1^2 - v_1\right) + \frac{0.42v_1^2}{2g}\frac{A_{base}^2}{A_{ejected}^2}\left(1 - \frac{d^2}{D^2}\right) \tag{2.5}$$

The syringe moved 55.8 μm per injection and the time taken is 40.8 μs. Therefore, as shown in Fig. 4, the flow speed at the front end of the piston is v_{base} = 1.37 m/s. The inner radius of the syringe at the front of the piston is R_{base} = 6.25 mm and therefore the inner cross-sectional area is A_{base} = 122.66 mm^2. The internal area of the syringe outlet is $A_{ejected}$ = 12.56 mm^2. The maximum length of the

ampoule is L = 62 mm and the kinematic number of water used at 20 ℃ is η = 1.044 × 10^{-6} m^2/s. By substituting the above values into equation (2.6), the pressure difference acting on the drug reservoir to be apllied to recharge the drug solution automatically can be calculated. This total pressure change $\triangle P_{total}$ might pushed the piston of the syringe-type drug reservoir and it had occurred after the drug escaped the upper drug chamber as the ball-check valve closed the drug chamber's neck simultaneously as well so that the pressure of the upper drug chamber becomes lower than the atmospheric pressure.

$$\Delta P_{total} = \Delta P_{syringe} + \Delta P_{sc} = 1.85 \times 10^{-5}\,\mathrm{Pa} \tag{2.6}$$

CHAPTER 3

Optimization of the microjet performance - Analysis

3.1 Assumptions and dominant variables

The check-valve system prevents air inflow from the outside, but at the same time, there is a chance the flow inside the nozzle may be interrupted. The pressure loss that occurs between the upper and lower drug chambers must be minimized. As shown in Fig. 2.5(a), about 20.4 us after the irradiation, the ball has moved down from the neck, and the microjet ejection occurred. The energy transferred to the liquid drug in the lower drug chamber can be expressed by Eq. (3.1), assuming that the moving ball mass transfer the kinetic energy to the drug. Additionally, the spring absorbs some of the energy as the ball pushes the spring as giving it displacement. One can represent the absorbed energy as a spring potential energy ($1/2kx^2$). Moreover, flow passes through between the nozzle neck and the ball from the upper chamber during the specific time $t_{elapsed}$, which is the time it takes for the ball to open and close the valve during the irradiation impulse. The third term on the right hand side of Eq. (3.1) is added assuming that there is a continuous flow as long as the nozzle neck is opened during a flow passage. Here, ρ_{water} (=1000 kg/m^3) is the density of drug solution, A_n (=3.142 mm^2) is the area of the nozzle neck, v_n (= 5 m/s) is the flow speed at the nozzle neck. We measured v_n = 5 m/s using the high-speed camera by tracking the trace particles (pigments) of size 0.25 - 0.50 μm inside the chamber.

$$E_{liquid} = \frac{1}{2} m_{ball} v_i^2 - \left\{ \frac{1}{2} k_s (\Delta x + \Delta l)^2 - \frac{1}{2} k_s \Delta l^2 \right\} + \frac{1}{2} (\rho_{water} A_n v_n t_{elapse}) v_n^2 \quad (3.1)$$

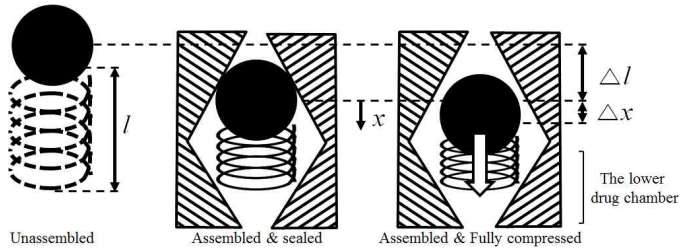

Fig. 3.1. Schematic of an original spring length, as assembled to a nozzle, and additionally compressed during the valve opens.

3.2 Modeling inside valve actuation

Here, E_{liquid} is the total energy harvested in the liquid drug, m_{ball} is the ball mass (0.11 g), v_i is the initial velocity of the ball, k_s is the spring coefficient, l is the original length of the spring, Δl is the initial displacement of the spring, x is the location of the ball attached to the spring and Δx is the maximum displacement of the compressed spring as illustrated in Fig. 3.1. Also, since the displacement is significantly less than the original length of the spring or $\Delta x << l$, Eq. (3.1) can be approximated as

$$E_{liquid} = \frac{1}{2} m_{ball} v_i^2 - k_s \Delta l \Delta x + \frac{1}{2} (\rho A_n v_n t_{elapse}) v_n^2 \tag{3.2}$$

In the lower drug chamber, the motion of the ball is assumed to be resisted by the drag force as in Eq. (3.3) from [12], such that

$$F_{drag} = cv^2 = c\left(\frac{dx}{dt}\right)^2 \tag{3.3}$$

The ball is surrounded by a converging-diverging wall and situated right next to a spring, which affects the flow conditions. Such complex arrangement makes it difficult to estimate the relevant Reynolds number which is essential in calculating the drag coefficient C_D. Thus, we have

adapted to the experimental values where the curve from Eq. (3.5) is fitted to the data points of maximum displacement of the ball. Adjusting the coefficient value, c = 1.271 kg/m. v is the velocity of the ball motion. Another resistive force by the spring is expressed by

$$F_{spring} = k_s \Delta l \tag{3.4}$$

Then the force balance of the overall drug chamber volume can be expressed by the following differential equation,

$$m_{ball} \frac{d^2 x}{dt^2} + c\left(\frac{dx}{dt}\right)^2 + k_s \Delta l = 0 \tag{3.5}$$

The equation is integrated with respect to time using the separation of variables, and the analytical expression of the ball location x with respect to t is obtained.

$$x = \alpha - \frac{m_{ball}}{2c} \log\left[\tan^2\left\{ \tan^{-1}\left(\sqrt{\frac{c}{k_s \Delta l}} v_i \right) - \left(\frac{\sqrt{c k_s \Delta l}}{m_{ball}} \right) t \right\} + 1 \right] \tag{3.6}$$

$$\alpha = \frac{m_{ball}}{2c} \log\left(\frac{c}{k_s \Delta l} v_i^2 + 1 \right) \tag{3.7}$$

This solution encompasses an oscillatory behavior as there are opposite direction of the spring force and the drag force against the initial ball direction. However, as can be seen in Fig. 3.1, there is a limit to the distance that the ball can move due to the shape of the nozzle. Therefore, there is a time range for the Eq. (3.5) such as $0<t<t_{elapse}$. At t = 0, the ball begins to move, and at $t = t_{elapse}$, the ball returns to its initial position and strikes the top nozzle neck. Within this time range, the ball stops its motion as it hits the nozzle neck before the oscillation occurs.

3.3 Simulation & experiment of inside valve actuation

The present work considered four different spring coefficients k_s, namely 12.68 N/m, 23.49 N/m, 40.07 N/m and 64.18 N/m. In particular, we chose five different initial displacements Δl of 5 mm, 7 mm, 9 mm, 11 mm, and 13 mm for the tests. Furthermore, the initial velocity v_i was set to 3 m/s as obtained from the high-speed recording of the ball motion during a single spring compression for each laser pulse. Figure 3.2 shows the displacement of the spring for four different spring coefficients by solving the Eq. (3.6). The pulsed motion of the elastic membrane opens the ball check valve while the spring is fully compressed and recovered during the time shown on the x-axis. The maximum value of each curve corresponds to the maximum displacement Δx of the spring during which the valve is open.

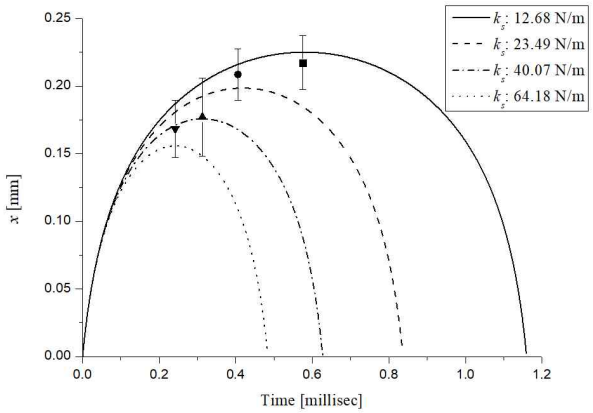

Fig. 3.2. Calculated displacement of spring, x, with time for four different spring coefficients ks of Δl = 5 mm. Rectangle is experiment of ks =12.68 N/m, circle is experiment of ks =23.49 N/m, triangle is experiment of ks =40.07 N/m, and inverted triangle is experiment of ks =64.18 N/m. Each case of experiment was performed 10 times and the range of the experiment value is indicated through the error bars.

Figure 3.3 shows the maximum additional displacement of the spring Δx, and the total energy harvested in the liquid drug E_{liquid} according to the spring constant k_s at the initial displacement of 5 mm. Here, Δx is the maximum of Eq. (3.6) and is a function of k_s. E_{liquid} is the value calculated from Eq. (3.2). E_{liquid} decreases as the spring constant k_s increases. Therefore, the ideal optimum value of k_s becomes zero, and such the energy transferred to the drug E_{liquid} has the maximum value for optimum performance.

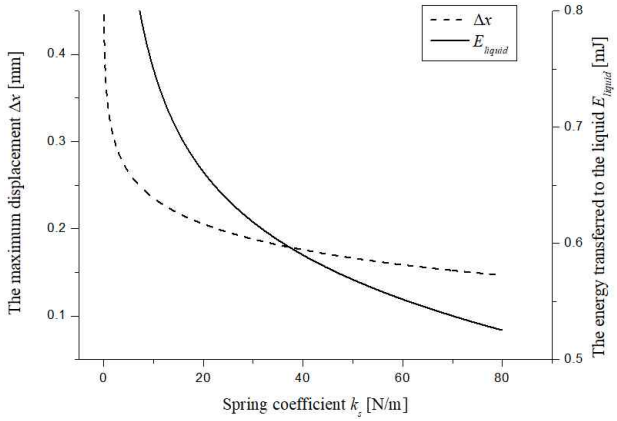

Fig. 3.3. Maximum additional displacement of the spring Δx (dash line), and the total energy harvested in the liquid drug Eliquid (solid line) according to spring constant ks for initial displacement of 5 mm

However, the spring constant k_s has a non-zero minimum. For each laser pulse irradiated at 10 Hz, the dynamic open-closure of the ball check valve must end within 0.1 seconds for a synchronization of nozzle chamber with the pressure chamber. Figure 3.4 shows the time elapsed ($t_{elapsed}$) for a single set of forward-backward motion of the spring, according to the spring coefficients. $t_{elapsed}$ is the time it takes for the ball to open and close the valve during the irradiation impulse. Solving Eq. (3.6) for x approaching zero gives the resulting value of $t_{elapsed}$. With decreasing spring coefficient, the time elapsed increases until reaching the laser pulse duration of the system at 10 Hz. This

suggests that if $t_{elapsed}$ exceeds 0.1 seconds, the ball check valve does not close, which eventually causes the outside air to flow into the nozzle outlet. The corresponding spring coefficient at which the time is 0.1s is found to be 0.002 N/m.

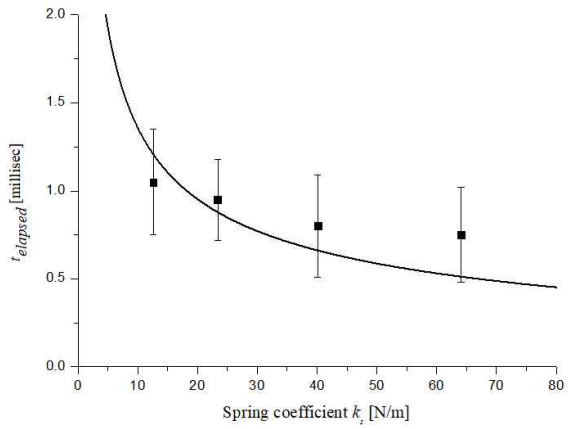

Fig. 3.4. Calculated time elapsed (telapsed, solid line) during which the valve opens and closes for various spring coefficients ks. Rectangle are experimental results (when ks = 12 N/m, 23.49 N/m, 40.07 N/m, 64.18 N/m). Each case of experiment was performed 10 times and the range of the experiment value is indicated through the error bars.

As the spring coefficient decreases, the maximum displacement of the spring Δx increases, all within the time duration of 0.1 seconds mentioned above. Effectively the energy transferred to the drug in the lower chamber increases and such the resulting microjet ejected out of the nozzle exit attains a higher speed. The experimental results shown in Fig. 3.5 demonstrate just that.

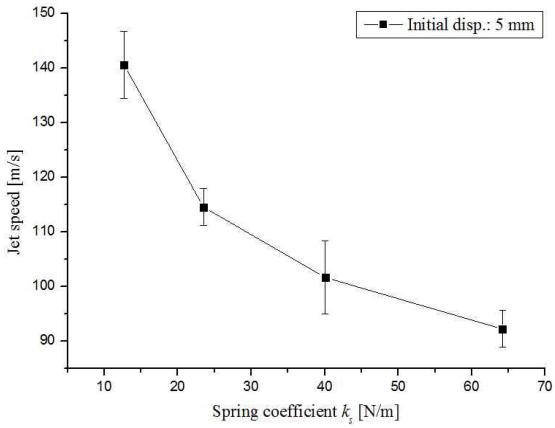

Fig. 3.5. Measured microjet speed according to spring coefficients for Δl = 5 mm. Each case of experiment was performed 10 times and the range of the experiment value is indicated through the error bars.

A similar analysis can be done for a fixed spring coefficient this time with varying original spring length. Figure 3.6 shows the displacement of the spring with respect to original spring lengths by solving Eq. (3.6). Figure 3.7 is the time elapsed ($t_{elapsed}$) for the corresponding spring initial displacement Δl. With the increasing length of the spring, the elapsed time decreases. At 0.1 second, the corresponding initial spring displacement Δl is 0.04 mm. With increasing Δl, the maximum displacement of the spring or the peak value of the curve decreases. Thus lower spring length increases the energy transferred to the drug in the lower chamber as shown in Fig. 3.8 and thus the speed of the microjets increases. The experimental results shown in Fig. 3.9 demonstrate just that. Noting the time elapsed must remain within 0.1 seconds as shown in Fig. 3.7, the optimum initial spring displacement is set to 0.001 mm.

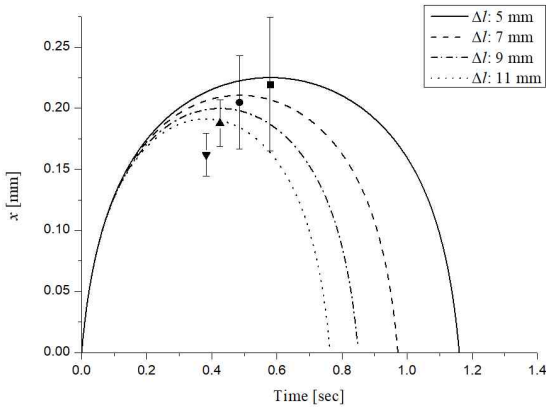

Fig. 3.6. Calculated displacement of the spring, x, with time for four different spring lengths. Spring coefficient ks = 12.68 N/m is considered. Rectangle is experiment of Δl = 5 mm, circle is experiment of Δl = 7 mm, triangle is experiment of Δl = 9 mm, and inverted triangle is experiment of Δl = 11 mm. Each case of experiment was performed 10 times and the range of the experiment value is indicated through the error bars.

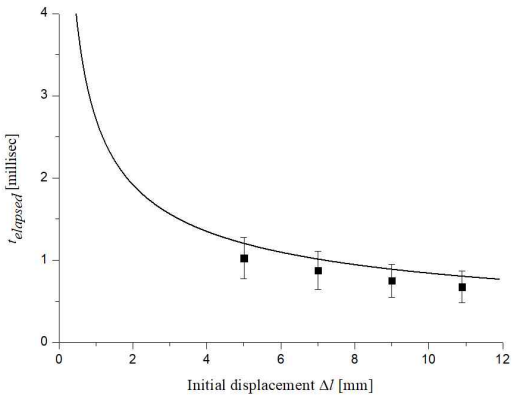

Fig. 3.7. Calculated time elapsed (telapsed, solid line) during which the valve opens and closes for varying initial spring displacements. Rectangles are experimental results (when Δl = 5 mm, 7 mm, 9 mm, 11 mm). Each case of experiment was performed 10 times and the

range of the experiment value is indicated through the error bars.

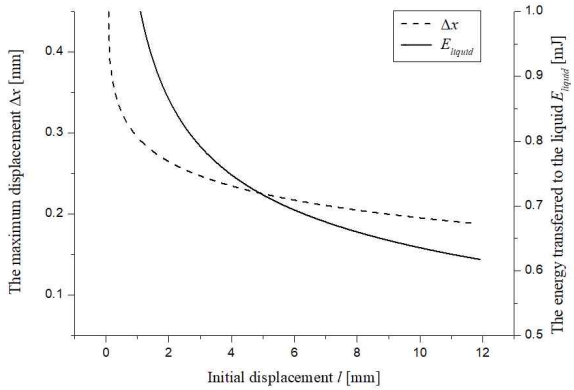

Fig. 3.8. Maximum additional displacement of the spring Δx (dash line), and the total energy harvested in the liquid drug Eliquid (solid line) according to the initial displacement Δl for spring coefficient of 12.68 N/m

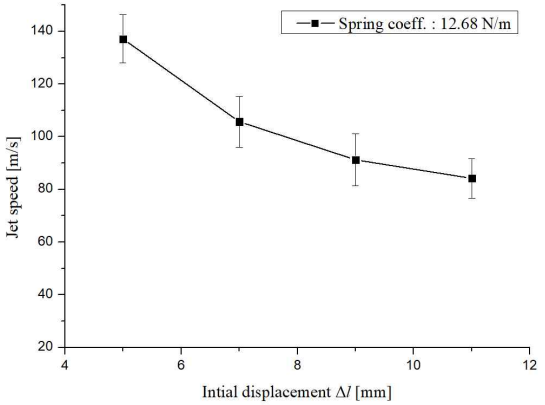

Fig. 3.9. Measured microjet speed according to initial spring displacement for spring coefficient of 12.68 N/m. Each case of experiment was performed 10 times and the range of the experiment value is indicated through the error bars.

CHAPTER 4

CONCLUSION

As an example of a flow generation actuator, a microjet drug delivery system discussed in a recent study injects a drug with a driving force of bubble expansion through a 10 Hz laser irradiation. However, the conventional microjet drug delivery system could not control the inflow from the outside of the nozzle synchronized with the pulsed power source, so that continuous operation was not possible. In this study, we implemented a nozzle opening/closing mechanism using a ball-check valve to control inflow in a microjet drug delivery system with a pulsed power source as described above. We compare the performance with existing microjet system and set the parameters to optimize the performance and maximize the energy delivered to the fluid through the check valve.

The injector with the ball-check valve prevented external air inflow which caused by a subsequent internal pressure drop after the drug release. This prevented the outside air from entering the nozzle while sustaining the penetration performance of repeated injection at a constant speed of 140 m/s.

The microjet speed was found to increase as the spring coefficient and the initial displacement of the spring were smaller. However, the smaller the coefficient, the more time the spring takes to return to its original state. When the recovery time exceeds the laser operation cycle of 0.1 second, an unnecessary bubble is formed in the lower drug chamber, so there is a limit of spring coefficient and initial displacement. Therefore, the optimum spring coefficient is 0.002 N/m

and the optimal initial displacement is 0.001 mm.

The drug penetration performance improved about 1.5 times to 2.25 times as compared with the case without ball-check valve. As the number of drug shots increases, the performance of microjets deteriorated and the penetration depth remained at 590 μm. However, the injector with ball-check valve maintained its performance. Therefore, as the number of drug shots (penetration time) increases, the penetration depth significantly increased to reach 1355 μm.

This finding is consistent with the fact that the flow inside the microjet drug delivery system using the laser is uniform for every pulse, and furthermore it is the development of the mechanism necessary for the design of a flow generator with a pulsed power source. The driving force is obtained by the pressure wave transmitted by the laser-induced bubble expansion. Since the laser operates at 10 Hz, the driving force is the form of 10 Hz pulse and generates pulsatile flow. Unlike a flow generator with a continuous driving force such as positive displacement pumps, speed pumps, and gravity pumps, a flow generator with a pulse-like driving force requires an automatic closing device that does not reduce the flow quality. Therefore, the ball-check valve proposed in this study could be a suitable solution and can be applied to the pulsatile flow devices such as a left ventricular assist device which requires pulsatile flow for a bridge to heart transplantation [17], an airblast injector in a reactive spraying system using high temperature, high-pressure flow [18], Atomization of gel propellants [19] in addition to laser-induced microjet drug injection

REFERENCES

[1] Claude A. Trépanier, Martin R. Lessard, Jacques G. Brochu, and Pierre H. Denault. 1990. Risk of cross-infection related to the multiple use of disposable syringes. Canadian Journal of Anaesthesia 37 (2): 156-9.

[2] Jeanne C. Stachowiak, Marcio G. von Muhlen, Thomas H. Li, Laleh Jalilian, Sapun H. Parekh, and Daniel A. Fletcher. 2007. "Piezoelectric control of needle-free transdermal drug delivery." Journal of Controlled Release 124 (1): 88-97.

[3] Andrew Taberner, Catherine Hogan, and Ian W. Hunter. 2012. "Needle-free jet injection using real-time controlled linear Lorentz-force actuators." Medical Engineering & Physics 34 (9): 1228-1235.

[4] Anubhav Arora, Mark R. Prausnitz, and Samir Mitragotri. 2008. Micro-scale devices for transdermal drug delivery. International Journal of Pharmaceutics 364 (2): 227-36.

[5] Jack J. Yoh, Hun-jae Jang, Mi-ae Park, Tae-hee Han, and Jung-moo Hah. 2016. A bio-ballistic micro-jet for drug injection into animal skin using a Nd: YAG laser. Shock Waves 26 (1): 39-43.

[6] Mi-ae Park, Hun-jae Jang, Fedir V. Sirotkin, and Jack J. Yoh. 2012. Er: YAG laser pulse for small-dose splashback-free microjet transdermal drug delivery. Optics Letters 37 (18): 3894-6.

[7] Hun-jae Jang, Eugene Hur, Yoonkwan Kim, Seol-Hoon Lee, Nae G. Kang, and Jack J. Yoh. 2014. Laser-induced microjet injection into preablated skin for more effective transdermal drug delivery. Journal of Biomedical Optics 19 (11): 118002-.

[8] Tae-hee Han, and Jack J. Yoh. 2010. A laser based reusable microjet injector for transdermal drug delivery. Journal of Applied Physics 107 (10): 103110.

[9] Tae-hee Han, Jung-moo Hah, and Jack J. Yoh. 2011. Drug injection into

fat tissue with a laser based microjet injector. Journal of Applied Physics 109 (9): 093105.

[10] George M. Hale, and Marvin R. Querry. 1973. Optical constants of water in the 200-nm to 200-μm wavelength region. Applied Optics 12 (3): 555-63.

[11] Ning H. Chen. 1979. An explicit equation for friction factor in pipe. Industrial & Engineering Chemistry Fundamentals 18 (3): 296-7.

[12] Frank M. White. 1999. Fluid Mechanics, WCB.

[13] Hamed Khatam, Chang Liu, and Krishnaswa Ravi-Chandar. 2014. Dynamic tensile characterization of pig skin. Acta Mechanica Sinica 30 (2): 125-32.

[14] John A. Gallagher, Aisling N. Annaidh, and Karine Bruyère. 2012. Dynamic tensile properties of human skin. Paper presented at IRCOBI Conference 2012, 12-14 September 2012, Dublin (Ireland),

[15] Peter Timmerman, and Jacobus P. van der Weele. 1999. On the rise and fall of a ball with linear or quadratic drag. American Journal of Physics 67: 538-546.

[16] Jesper Ankersen, Alexander E. Birkbeck, Robert D Thomson, and Peter Vanezis. 1999. Puncture resistance and tensile strength of skin simulants. Proceedings of the Institution of Mechanical Engineers.Part H, Journal of Engineering in Medicine 213 (6): 493-501.

[17] Francis D. Pagani, Leslie W. Miller, Stuart D. Russell, Keith D. Aaronson, Ranjit John, Andrew J. Boyle, John V. Conte et al. 2009. Extended mechanical circulatory support with a continuous-flow rotary left ventricular assist device. Journal of the American College of Cardiology 54 (4): 312-321.

[18] Wayne Strasser. 2011. Towards the optimization of a pulsatile three-stream coaxial airblast injector. International Journal of Multiphase Flow 37 (7): 831-44.

[19] Victor Chernov, and Benveniste Natan. 2006. Atomization of gel propellants using pulsatile injection. ICLASS-2006 Kyoto Japan.

초 록

본 연구에서는 펄스 형태를 가지는 구동력에 자동적으로 반응하는 노즐 클로저를 개발하였으며 유동이 발생할 때 노즐을 개방시키고 유동이 발생하지 않을 경우 노즐을 폐쇄하여 불필요한 공기 유입을 방지하도록 하였다. 본 연구에서 다루는 인젝터에 ball check valve 노즐 클로저를 부착시킨 인젝터와 그렇지 않은 인젝터의 약물 침투 성능을 다양한 방법으로 비교하고 분석하였다. 노즐 클로저는 발사 횟수에 상관없이 지속적인 성능을 유지시키며 노즐클로저가 약물 발사 후 인젝터의 노즐을 폐쇄하므로 분사된 약물의 양만큼의 약물이 외부 시린지에서 자동으로 충전된다. 노즐 클로저가 부착되지 않았을 경우의 마이크로젯 속도의 97 %에 달하며 약물 침투 깊이가 경우에 따라 약 1.5배에서 2.25배 더 향상됨을 확인할 수 있었다. 또한 이러한 마이크로젯 성능에 대한 주요 변수를 설정하여 해석하고 system을 최적화 하였다.

주요어 : 마이크로젯, 레이저 유도 버블 (Laser-induced bubble), Ball-chenck valve, Needle-free, Drug-delivery, Jet injection

학번 : 2016-20759